Toward New Benchmark Adsorbents: Preparation and Characterization of Activated Carbon from Argan Nut Shell for Bisphenol A Removal

Mohamed ZBAIR[1,2,3,*], Kaisu AINASSAARI[2], Asmaa DRIF[1], Satu OJALA[2], Michael BOTTLINGER[3], Minna PIRILÄ[2], Riitta L. KEISKI[2], Mohammed BENSITEL[1], Rachid BRAHMI[1,*]

[1]*Laboratory of Catalysis and Corrosion of Materials (LCCM), Department of Chemistry, Faculty of Sciences of El Jadida, University of Chouaïb Doukkali, BP.20, 24000 El Jadida, Morocco.*

[2]*Environmental and Chemical Engineering, Faculty of Technology, P.O. Box 4300, FI-90014 University of Oulu, Finland.*

[3]*Laboratory of Hydrothermal Carbonization Process, Umwelt-Campus Birkenfeld, Trier University of Applied Sciences, Germany.*

**Corresponding authors: zbair.mohamed@gmail.com , rbrahmi1997@gmail.com*

This is a post-peer-review, pre-copyedit version of an article published in Environmental science and pollution research. The final authenticated version is available online at: http://dx.doi.org/10.1007/s11356-017-0634-6

Abstract

The use of argan nut shell as a precursor for producing activated carbon was investigated in this work. Two activated carbons AC-HP and AC-Na were prepared from argan nut shell by chemical activation method using phosphoric acid (H_3PO_4) and sodium hydroxide (NaOH), respectively. Textural, morphological and surface chemistry characteristics were studied by nitrogen physisorption, TGA, SEM, TXRF, FTIR, XRD, and by determining the

pH_{PZC} of the AC-HP. The adsorption experiments revealed that AC-HP was more efficient in adsorption of BPA due to high specific surface area (1372 m^2/g) compared to AC-Na (798 m^2/g). The obtained adsorption data of BPA on AC-HP correlated well with the pseudo-second-order model and the Langmuir isotherm (Qmax= 1250 mg/g at 293 K). The thermodynamic parameters ($\Delta G°<0$, $\Delta H°<0$, and $\Delta S°<0$) indicate that adsorption of BPA on AC-HP was spontaneous and exothermic in nature. The regeneration of AC-HP showed excellent results after 5 cycles (95 %- 93%). This work does not only provide a potential way to use argan nut shell, but also represents a sustainable approach to synthesize AC-HP, which might be an ideal material for various applications (energy storage, catalysis and environmental remediation).

Keywords: Activated carbon; Argan nut shell; Chemical activation; Adsorption; Bisphenol A.

1. Introduction

Bisphenol A, 2,2-bis-(4-hydroxyphenyl) propane (BPA), is a basic organic chemical used as a raw material to produce polycarbonate plastics and epoxy resins. BPA is known as an endocrine upsetting substance (EDC) and it is delegated xenoestrogen. EDCs cause physiological impacts since they resemble the natural hormone and can interfere with hormone production, release, metabolism and elimination (Selvaraj et al., 2014). Because of the earlier wide use of BPA, there is an increasing interest to discover viable remediation technology for its destruction in wastewaters. Bisphenol A has been detected in a wide range of natural waters. The maximum concentrations observed is reaching up to 0.1 g/L in drinking water (Ono, 2000), 12 g/L in stream water (Kolpin et al., 2002) and 17.2 mg/L in risky waste landfill leachates (Yamamoto et al., 2001). Late results showed that bisphenol A is related to estrogenic action at a low dose of 0.23 pg/mL in a culture medium (Wetherill et al., 2007). Numerous in vitro and in vivo assays have affirmed that bisphenol A increase the genital tract abnormalities, the incidence of infertility and breast cancer (Howdeshell et al., 1999; Muñoz-de-Toro et al., 2005).

Nowadays, different removal methods have been utilized for the BPA removal. For instance photocatalytic degradation is able to achieve BPA removal of 79% for 20 mg/L of BPA after 3 hours (Pirilä et al., 2015). Ozonation method also achieves high removal (>99%) of BPA (Alum et al., 2004). Another popular treatment method used by many researchers is adsorption using activated carbon, one of the oldest water treatment methods (Dias et al., 2007; Rivera-Utrilla et al., 2011). In a previous study, six types of powdered activated carbon (PAC) were tested, and the result was that 31 to 99% of BPA could be removed using 5 and 15 mg/L of activated carbon dosage (Yoon et al., 2003). The chemical and textural surface properties are the important characteristics of activated

carbons, including the high surface area and the type of the functional groups present on the activated carbon surface (Moreno-Castilla and Rivera-Utrilla, 2001).

Activated carbons can be produced from different types of raw materials by physical or chemical activation or by combination of both. In this purpose, we conducted research to explore the possibility of producing activated carbon from argan nut shells. The argan nut shells (from Argania spinose) are generated as agricultural waste during the argan oil extraction. Argania spinosa is endemic tree and covering a wide area of 828,000 ha in Morocco and the annual argan oil production is 6000 tons producing 2700 tons argan shell waste per year. Currently the local population uses the argan shell waste as a heating fuel. However, this biomass could be used also as a renewable resource in the preparation of activated carbon similarly to coconut shell, almond or olive pomace. There exist also earlier studies that use argan nut shells as the raw material of activated carbons prepared by chemical activation using K_2CO_3 and KOH as activating agent. The specific surface areas obtained for these materials were 527 and 682 m^2/g, respectively (Chafik, 2012).

The principal objective of this study was to valorize argan nut shell (RM) to prepare activated carbon with higher specific surface area than before by using phosphoric acid (H_3PO_4) and sodium hydroxide (NaOH) as activating agent. The potential practical application of the prepared activated carbons (AC-HP and AC-Na) in adsorption of bisphenol A was as well evaluated.

2. Materials and methods

2.1. Reagents

The activating chemicals used were phosphoric acid H_3PO_4 (purity >99%) and sodium hydroxide NaOH (purity 98%). Bisphenol A (purity 99%), BPA (Fig. 1) were purchased from Sigma Aldrich.

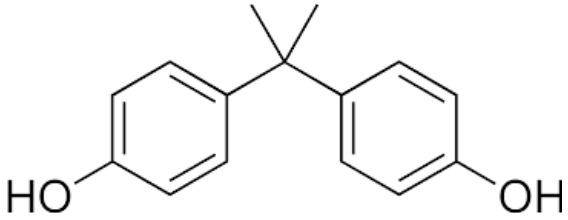

Fig. 1. Molecular structure of Bisphenol A (BPA).

2.2. Preparation of activated carbons

The preparation process consists of the carbonization of argan nut shell under nitrogen atmosphere followed by chemical activation using H_3PO_4 and NaOH. The carbonization of argan nut shell (RM) was performed under a continuous flow of purified nitrogen gas with a flow rate of 60 mL/min. The precursor was heated from room temperature to 550 °C (10 °C/min) and maintained at this final temperature for 60 min. The activation of the obtained char was then achieved by treating the char at room temperature with activating chemicals having the mass ratio of 1. Next, the resulting slurry was dried. The dried slurry was then placed in the reactor and pyrolyzed at 700 °C for 1 hour under a nitrogen flow (60 mL/min). Finally, the samples were washed and then dried at 120 °C. Activated carbons prepared by H_3PO_4 and NaOH were labeled as AC-HP and AC-Na, respectively.

2.3. Characterization of activated carbons

Thermo-gravimetric analysis (TGA) aimed to identify the principal temperature levels at which the nut shell of argan reacts under an inert atmosphere. Thermal analyses were carried out with STD 2960 TA and SDT Q600 instruments under a nitrogen flow of 100 mL/min. The temperature ramp of 5 °C/min from room temperature to 1000 °C was used during the analyses.

The crystalline structure of AC-HP and AC-Na were examined by X-ray diffraction (XRD) analysis (Bruker-eco D8 Advance diffractometer). The interlayer spacing d_{hkl} of AC-HP and AC-Na was determined using the Bragg equation:

$$d = \frac{\lambda}{2}\, sin\theta \quad (1)$$

Where: θ corresponds to the scattering angle of each peak; λ = 0.154 nm is the X-ray length. The crystallite width along the a-axis (L_a), and (L_c) crystallite height along the C-axis, were determined using this equation (Marsh and Rodríguez-Reinoso, 2006; Post, 1975):

$$L = \frac{K\lambda}{B}\, cos\theta \quad (2)$$

Where: L corresponds to (L_c) or (L_a) and B is the full width half maximum of the peak (FWHM). While (L_c) and (L_a) calculation, the peaks (0 0 2) and (1 0 0) were used and K is equal to 0.9 and to 1.84, respectively.

The effective dimension (L') of the graphitic microcrystallites was calculated using the following equation (Emmerich and Luengo, 1993):

$$L' = \left(\frac{\pi}{4}\right)[L_a^2 L_c] \quad (3)$$

The N2 adsorption-desorption isotherms of AC-HP and AC-Na were measured using a Micromeritics ASAP 2020 instrument to determine surface area, pore volume, and pore size distribution.

The morphological characteristics of argan nut shell (RM), AC-HP and AC-Na were analyzed using a Field Emission Scanning Electron Microscopy ZEISS ULTRA plus.

The quantification of element concentrations in the raw material (RM) and activated carbon was done by using an S2 PICOFOX TXRF (Bruker AXS Microanalysis). Before analysis, around 100 mg of sample was grounded in a mortar and then suspended in a detergent solution of standard (Se) with concentration of 30 mg/L.

The PZC (point of zero charge) of AC-HP was determined using the pH drift method (Mohan et al., 2011; Noh and Schwarz, 1989). 0.20 g of AC-HP was mixed with 50 mL of 0.01 M NaCl solution. The pH of the starting solutions (2.0 to 12.0) was adjusted using HCl and NaOH. After 24 h, the final pH was measured.

The functional surface groups of the argan nut shell (RM), AC-HP and AC-Na, were determined using a Fourier Transformed Infrared spectroscopy (FTIR–8400S, Shimadzu).

2.4. Batch adsorption experiments

The batch tests were conducted to evaluate the effect of temperature (293-333 K) and pH (2.0-12.0) on the adsorption rate of bisphenol A (BPA). In each experiment, 200 mL of BPA solution (60 mg/L) was placed in a 250 mL Erlenmeyer flask. Then, 0.01 g of adsorbent was added to the solution. The AC-HP and AC-Na was separated from the solution by filtration using a 0.2 µm millipore filters (polyether sulfon membrane; VWR-USA). The residual BPA concentration in the liquid-phase was analyzed by using a UV/Vis spectrophotometer (Beckman DU-640i spectrophotometer, USA) at the maximum absorbance wavelength (λ_{max}) of 274 nm. Kinetics of adsorption was determined by

analyzing the removal of BPA from an aqueous solution at different time intervals. Adsorption equilibrium experiments were carried out at different temperatures (293, 303, and 313 K, respectively) by agitating 0.01 g of AC-HP and 200 mL of BPA solution with different concentrations (10-60 mg/L) for 3 h.

2.5. Adsorption modelling

2.5.1. Calculations

The amount of BPA adsorbed per unit mass of AC-HP and AC-Na Q_t (mg/g) at certain time *t*, was calculated using the following equation:

$$Q_t = \frac{(C_i - C_t)V}{m} \quad (4)$$

The BPA removal percent (%) was calculated according to Eq. (5):

$$Removal\ (\%) = \frac{(C_i - C_t)100}{C_i} \quad (5)$$

The adsorption kinetics of BPA onto AC-HP was investigated using the Pseudo-First-Order, Pseudo-Second-Order and Intra-particle diffusion models (McKay, 1999; Laabd et al., 2016; Weber, W.J. and Morris, 1963). Then, the adsorption isotherm data were fitted to the Langmuir and Freundlich models (Langmuir, 1916; Freundlich, 1906). Also, the thermodynamic parameters were calculated using the Van't Hoff and Gibbs-Helmholtz equations (Han et al., 2011). The equations of these models are summarized in Table 1.

Table 1 Kinetics, isotherm models and thermodynamic equations.

Equation name	Equations	Description	Ref.
Pseudo-First-Order	$ln\,(Q_e - Q_t) = ln\,Q_e - K_1 t$	Q_e and Q_t are the adsorbed BPA amounts at equilibrium and at times t, respectively. K_1: the rate constant.	(McKay, 1999)
Pseudo-Second-Order	$\frac{t}{Q_t} = \frac{1}{K_2\ Q_e^2} + \frac{t}{Q_e}$	K_2: rate constant	(Laabd et al., 2016)
Intra-particle diffusion	$Q_t = K_i t^{0.5}$	K_i: rate constant	(Weber, W.J. and Morris, 1963)
Langmuir	$\frac{1}{Q_e} = \frac{1}{(K_L Q_{max})C_e} + \frac{1}{Q_{max}}$	C_e and Q_e are the concentration and amount at equilibrium; K_L: direct measure of the intensity of the adsorption process; Q_{max}: maximum adsorption capacity.	(Langmuir, 1916)
Adsorption feasibility	$R_L = (1 + K_L C_0)^{-1}$	R_L: adsorption process mode, if the process is unfavorable (R_L>1), linear (R_L=1), favorable (0<R_L<1), or irreversible (R_L=0) (C_0 is the highest initial BPA concentration)	(Kubilay et al., 2007)
Freundlich	$ln\ Q_e = \frac{1}{n} ln\ C_e + ln\ K_F$	K_F: adsorption capacity; n: intensity of adsorption; 1/n=0 irreversible; 1/n>1 unfavorable 0<1/n<1 favorable.	(Freundlich, 1906)
Gibbs free energy	$\Delta G^\circ = -RTlnK_d$	ΔG°: Gibbs free energy change; K_d: equilibrium constant; R: gas constant; T: temperature.	(Han et al., 2011).
Van't hoff	$lnK_d = \frac{\Delta S^\circ}{R} - \frac{\Delta H^\circ}{R.T}$	ΔS°: entropy change; ΔH°: enthalpy change.	(Han et al., 2011).

3. Results and discussion

3.1. Characterization of activated carbons

3.1.1. TGA-DTG analysis

The thermo-gravimetric analysis provides information on the thermal behavior of the argan nut shell (raw material). The TG curve shows a mass loss in the range of 18–1000 °C, which can be divided into several steps as shown in Fig. 2. In the figure, the relative mass loss (TGA) and their first derivative (DTG) curves are presented for a dried argan nut shell. The endothermic mass loss (11.10 wt %) observed at temperatures lower than 120 °C can be attributed to water desorption. The second mass loss (28.89 wt %) between 120 °C and 190 °C is associated to the decomposition of organic substances. Beyond this temperature, thermal degradation of the main components of the biomass begins: between 190 °C – 320 °C the hemicellulose fraction is degraded, followed by the degradation of cellulose between 320 °C – 400 °C and lignin above 400 °C (56.66 wt %) (Orfão et al., 1999). The argan nut shell has an average fiber content of 69.73 % (including cellulose, hemicelluloses, lignin), which suggests this waste biomass to be suitable for obtaining carbonaceous material (McKendry, 2002). Stabilization of the material was observed above 550 °C. Based on this result; the selected pyrolysis temperature to obtain carbonaceous material was 550 °C.

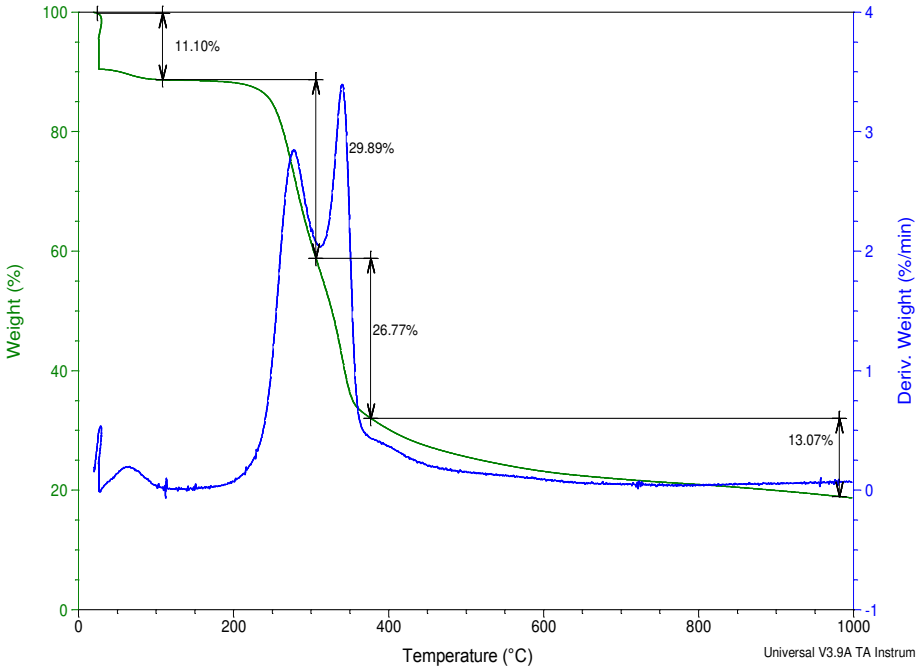

Fig. 2. TGA-DTG diagram of the argan nut shell under argon atmosphere.

3.1.2. X-Ray diffraction analysis

Fig. 3 shows the XRD patterns of AC-HP and AC-Na. From Fig. 3 two diffraction peaks at around 24° and 43° can be observed. These peaks are related to the (0 0 2) and (1 0 0) graphite-like reflections (Hadoun et al., 2013; Suhas et al., 2017). The peak at 2θ = 24°, having higher intensity, results from the stacks of parallel layers and the values of the interlayer spacing, d_{002}, are listed in Table 2. The distance of the (0 0 2) plane is in the range of 0.359–0.366 nm. However, it should be noted that this value is greater than that of graphite (0.335 nm) and that framework is still disordered and far from the complete graphitization (Hadoun et al., 2013). The peak at 2θ of 43° is assigned to the regular structure within the individual layer plan segments (Ignat et al., 2010). This type of a model (Fig. 3) is known to be characteristic for the carbon states described as disorganized carbon (Davydov et al., 2004). L_c and L_a determined from the intensity of the peaks (0 0 2) and (1 0 0) are shown in Table 2. From this table, it is found that the variation of (L_c) is less pronounced and (L_a) increases from 6.97 to 9.39, which can be

explained by the growth of the crystallites in the plane and the existing graphite-like layers develop through the incorporation of unorganized carbon. The crystallite of AC-HP and AC-Na growth in the plane results only from an increase in L_a. The dimension (L_c) and the number of crystallites do not change (Hadoun et al., 2013).

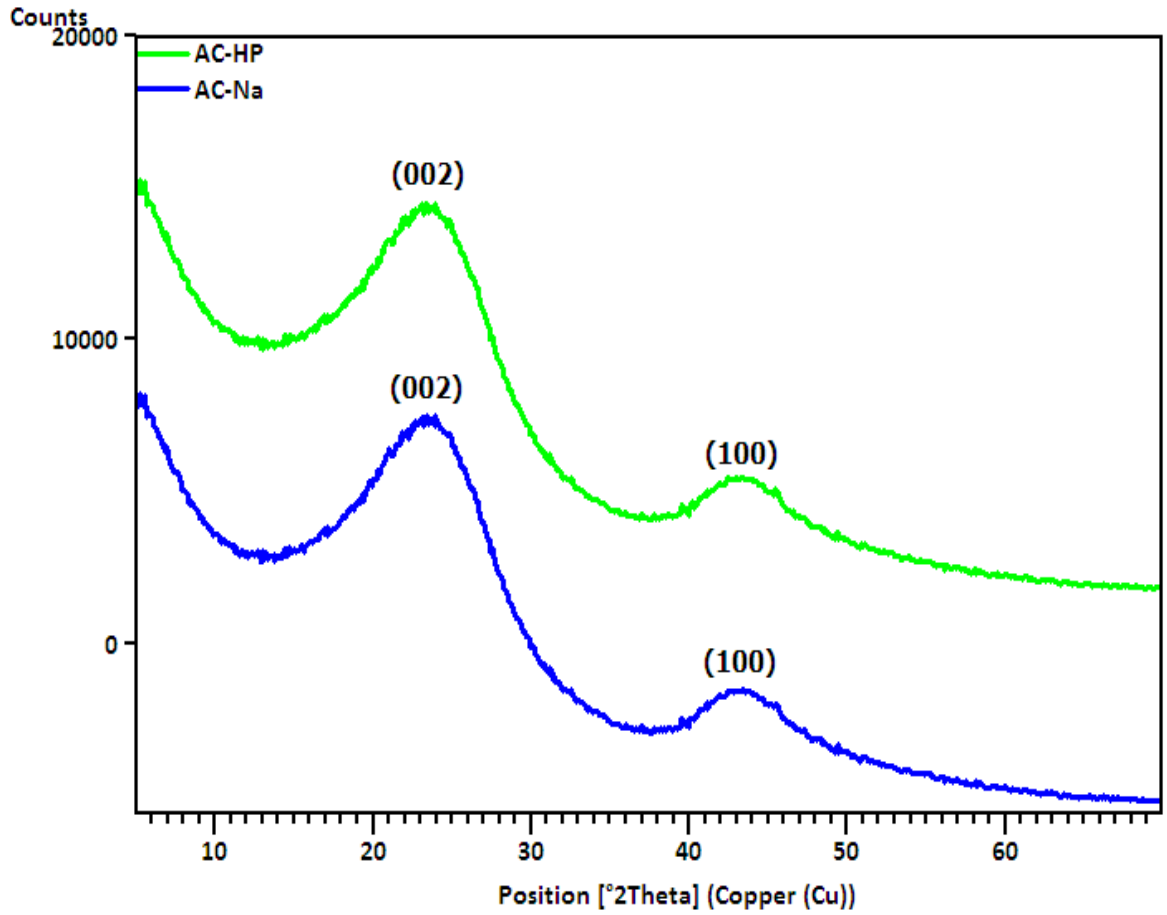

Fig. 3. XRD patterns of AC-HP and AC-Na.

Table 2 Interlayer spacing and microcrystallite parameters of AC-HP and AC-Na.

Samples	X-ray Data				Microcrystallite Parameters (nm)		Effective Dimension (nm)
	$2\theta_{002}$ (deg.)	$2\theta_{100}$ (deg.)	d_{002} (nm)	d_{100} (nm)	L_c	L_a	L'
AC-HP	24.77	43.27	0.359	0.208	8.98	6.97	5.95
AC-Na	24.85	43.86	0.366	0.206	8.52	9.39	7.13

3.1.3. Nitrogen physisorption analysis

The textural properties of the AC-HP and AC-Na were measured by nitrogen physisorption at 77 K. It was evident that both AC-HP and AC-Na presented the Type I physisorption isotherm (Fig. 4) (Sing et al., 1985), which is characteristic for the microporous materials. The results show that the H_3PO_4 allowed to obtain the highest specific surface area, highest pore volume and narrow pore size distribution (Table 3). These properties offer a good potential for the prepared activated carbons to be used as efficient adsorbents. Table 4 show a comparison of various activated carbons prepared by chemical activation from argan nut shell. The adsorbents prepared in this work showed relatively higher surface area (1372 m^2/g), compared to certain previous works reported in the literature.

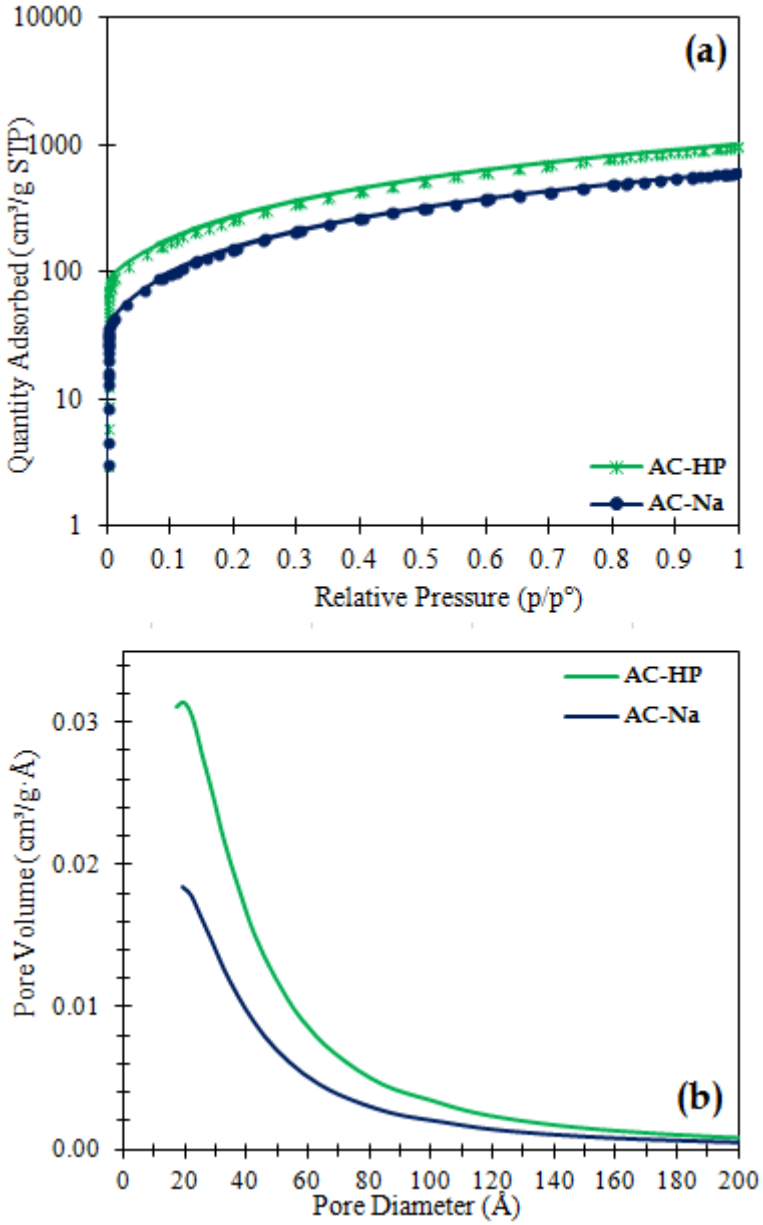

Fig. 4. Nitrogen physisorption isotherm and pore size distributions for AC-HP and AC-Na.

Table 3 Textural properties of the activated carbons prepared.

Activated Carbon	BET Surface Area (m^2/g)	Langmuir Surface Area (m^2/g)	Total Pore Volume (cm^3/g)	Average Pore Diameter (nm)
AC-HP	1372	929	1.50	1.70
AC-Na	798	546	0.90	1.92

Table 4 Comparison of surface areas of various activated carbons prepared from argan nut shell.

Chemical Activation Agent	BET Surface Area (m^2/g)	Reference
KOH	682	(Chafik, 2012)
K_2CO_3	527	(Chafik, 2012)
H_3PO_4	1372	Our study
NaOH	798	

3.1.4. Scanning electron microscopy (SEM)

SEM images (Fig. 5) show that the raw material (RM) had a relatively smooth surface with no porosity, except some occasional cracks. In contrast, the morphology of activated carbons indicates substantial changes on the surface porosity provoked by the chemical activation. Furthermore, the activating agent H_3PO_4 seems to increase the surface roughness more than the activating agent NaOH. This development of porosity is in good agreement with the results shown in textural properties (Table 3).

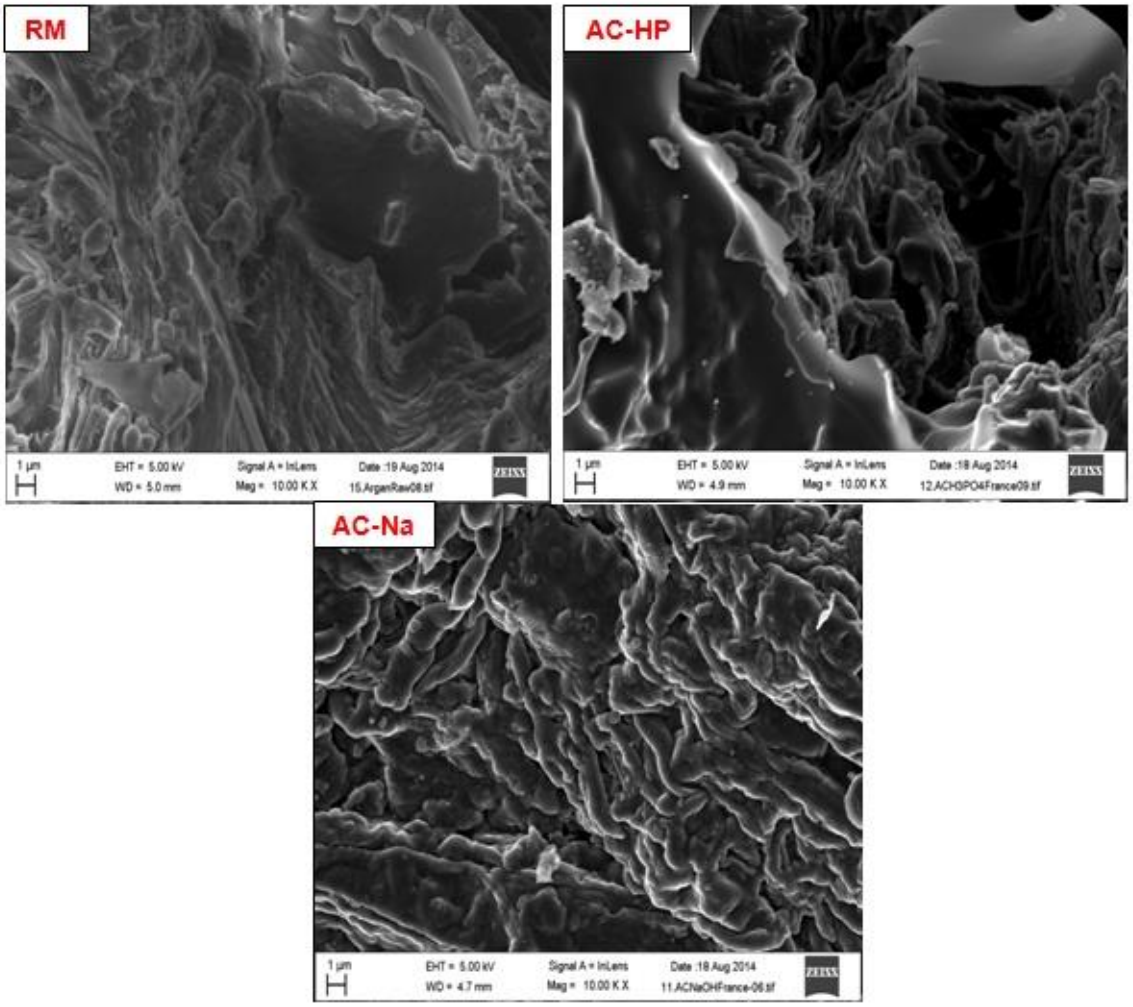

Fig. 5. FE-SEM images of argan nut shell (RM), AC-HP and AC-Na.

3.1.5. Total reflection X-ray fluorescence (TXRF)

The inorganic composition of AC-HP and AC-Na were analyzed with TXRF and are shown in Table 5. The inorganic composition was high in the samples analyzed. Phosphorus (P) concentration was the highest in AC-HP and sodium (Na) concentration was higher in AC-Na. The highest concentration of P and Na concentration is coming from H_3PO_4 and NaOH used during activation process (Lillo-Ródenas et al., 2001).

Table 5 Impurities content in RM, AC-HP and AC-Na.

Element	Unit	Sample Code		
		RM	AC-HP	AC-Na
Al	mg/kg	142	114	n.d.
Mg		214	147	667
P		562	1208	122
S		288	82	144
Cl		663	13	6
K		1771	704	593
Na		25427	22290	38666
Ca		1524	657	250
Mn		6	7	2
Fe		186	145	92
Ni		0.47	0.42	0.45
Cu		2	3	1.03
Zn		7	4	5
As		0.43	n.d.	n.d.
Se(IS)		100	100	100
Br		2	0.14	0.22

n.d: not detected

3.1.6. Fourier transformer infrared spectroscopy (FTIR)

FTIR spectrum shown in Fig. 6, reveals that argan nut shell presents the IR band at around 3436 cm^{-1}, which is related to the υ(O-H) vibrations in the hydroxyl groups. The band located at around 2923 and 2852 cm^{-1} corresponds to the υ(C-H) vibrations in methyl and methylene groups (El-Nabarawy et al., 1997; Figueiredo et al., 1999). Furthermore, the band appearing at 1740 cm^{-1} could be assigned to the C=O stretching vibrations in ketones

(RCOR') or carbonyl groups (C=O). The aromatic C=C bonds correspond to the peak at 1636 cm^{-1}. The peak located at 1510 cm^{-1} is assigned to the C=C ring stretch of aromatic rings (Bouchelta et al., 2008). Besides, the band located at 1458 cm^{-1} confirms the presence of the C=C of aromatic rings (Deng et al., 2010). In addition, the sharp peak observed at 1384 cm^{-1} could be attributed to the υ(C-O) vibrations in carboxylate groups. Furthermore, the bands observed between 1300 and 900 cm^{-1} might be assigned to the C-O stretching vibrations. The IR band located at 571 cm^{-1} attributes to the in-plane ring deformation (Ji et al., 2007). The FTIR spectra of AC-HP and AC-Na are similar, and the intensity of the bands at 2923 and 2852 cm^{-1} are decreased compared to the argan nut shell. Besides these peaks, the bands at 3436, 1636 and 571 cm^{-1} in the activated carbons was quite similar to those of the raw material. Hence, the other peaks were disappeared. This indicated that almost of surface functional groups were removed during the chemical activation process in AC-HP and AC-Na. The FTIR results agree with the surface chemistries of other agricultural by-products, such as raw cashew nut shell and Pecan Nutshell (Udeye, 2009; Vaghetti et al., 2009).

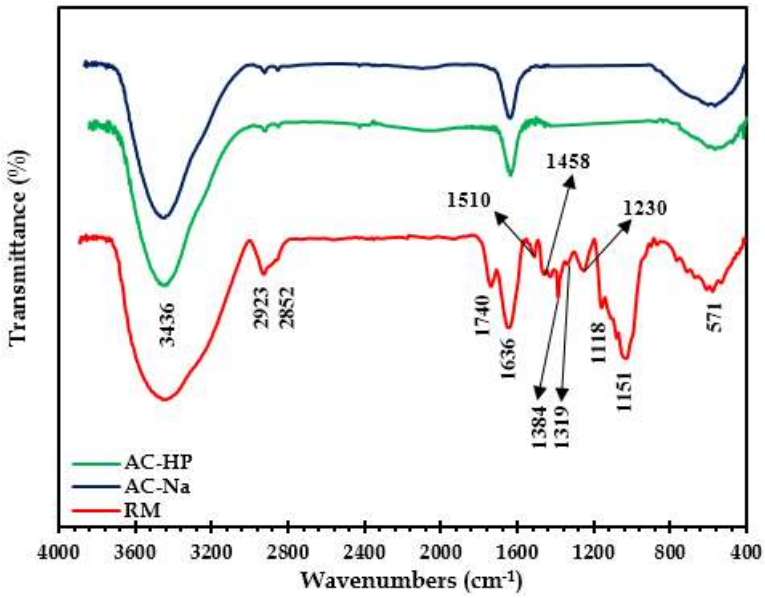

Fig. 6. FTIR spectra of raw material, AC-HP and AC-Na.

3.2. BPA adsorption studies

3.2.1. BPA removal by AC-HP and AC-Na

Preliminary adsorption tests on AC-HP and AC-Na were performed in order to find out the BPA removal capability. It can be observed in Fig. 7 that AC-HP had a higher BPA adsorption potential than that of AC-Na. This might be due to the higher specific surface area of AC-HP than AC-Na. Henceforth; the further batch experiments were performed to evaluate the BPA adsorption characteristics of AC-HP only.

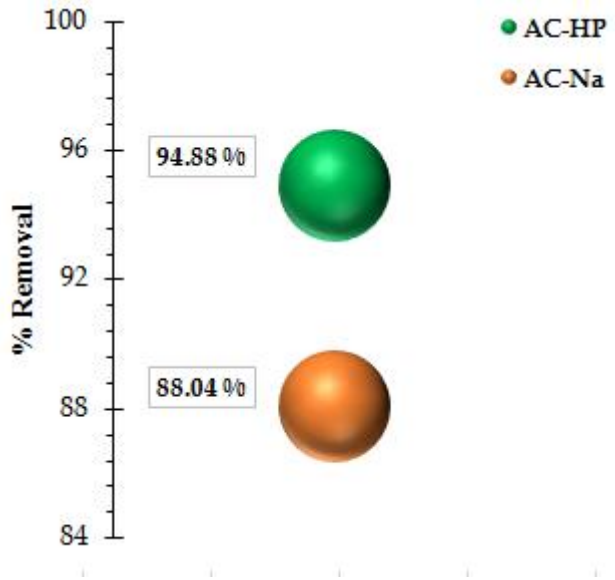

Fig. 7. Results of preliminary adsorption tests of the removal of BPA by AC-HP and AC-Na (C_0=60 mg/L; m= 0.01 g; stirring speed=200 rpm).

3.2.2. Effect of pH of the solution

The effect of the initial pH on the BPA removal was evaluated using 0.01 g of AC-HP, initial concentration of BPA of 60 mg/L, contact time for 3 h at room temperature. As shown in Fig. 8, the BPA removal was relatively constant from pH 2 to 8. However, the removal rate decreased when pH increased from 8 to 12. The reduction of the removal rate of BPA by AC-HP occurs at very basic pH range (>8.0). This result is due to the surface charge density of AC-HP and to the charge of bisphenol-A species both of which are depending on the pH of the solution. For this reason, the PZC study of AC-HP was performed.

Fig. 9 shows that the pH_{PZC} of AC-HP is 7.0. At this pH, the pH of a solution being similar to the pH_{PZC} value of carbon, the net surface charge density of activated carbon is near to zero, and this enhances the л-л dispersion interaction. Consequently, when the solution pH is 8.0 and above, the surface charge density of AC-HP is negative and bisphenol A is deprotonated (Sui et al., 2011). As a result, the repulsive electrostatic interaction is intensified. This was the main mechanism that contributed to the weak adsorption efficiency of BPA onto AC-HP at pH> 8.0. These results were consistent with the previous research on adsorption of BPA onto activated carbon (Bautista-Toledo et al., 2005; Tsai et al., 2006).

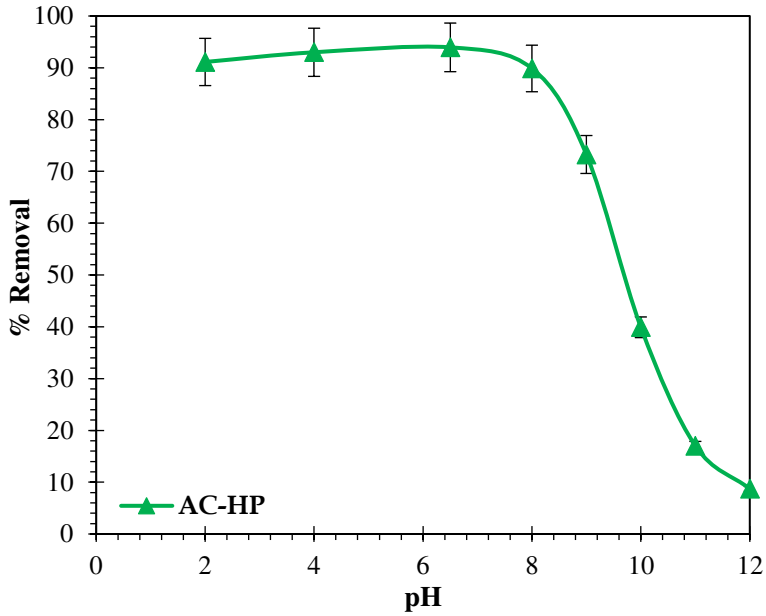

Fig. 8. Effect of initial pH on adsorption of BPA onto AC-HP.

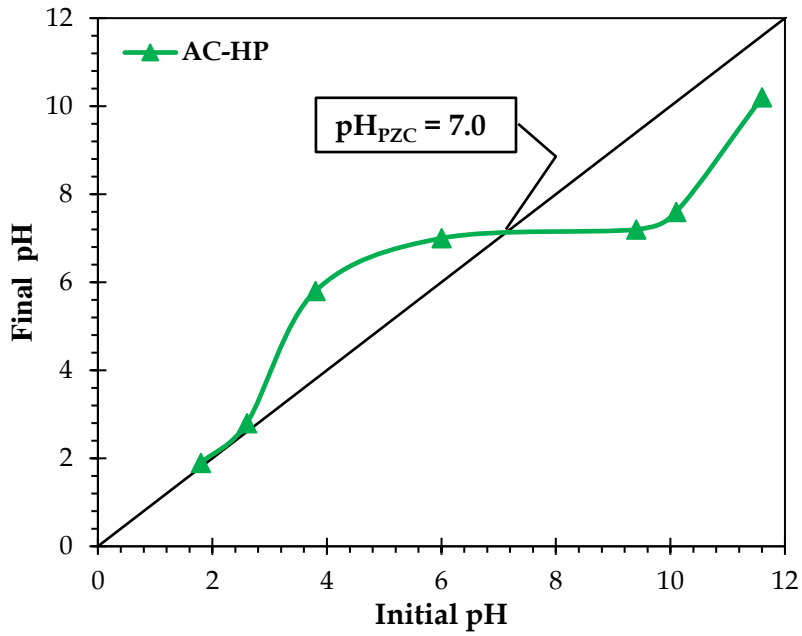

Fig. 9. pH_{PZC} (point zero charge) of AC-HP.

3.2.3. Effect of temperature

Different parameters related to the adsorbent and the BPA can influence the kinetics of adsorption by AC-HP among them, the temperature. In this context, three different temperatures were selected: 293 K, 313 K and 333 K for the experiments to study their effect on contact time and the adsorption capacity. As shown in Fig. 10, the adsorption capacity of AC-HP decreased by increasing temperature. The adsorption of BPA decreased from 1088 mg/g to 754 mg/g. The decrease in the adsorption of BPA may be due to desorption caused by an increase in the available thermal energy. This changes the position of the adsorption-desorption equilibrium. Also, the BPA adsorption was rapid in the initial stages of the removal process. After 60 min, the adsorption capacity did not change significantly up to 180 min leading to equilibrium. The fast-initial adsorption rate may be attributed to a large surface area of AC-HP as inferred from the BET surface area. The rapid establishment of the equilibrium is beneficial for the application of AC-HP in the removal of pollutants at room temperature.

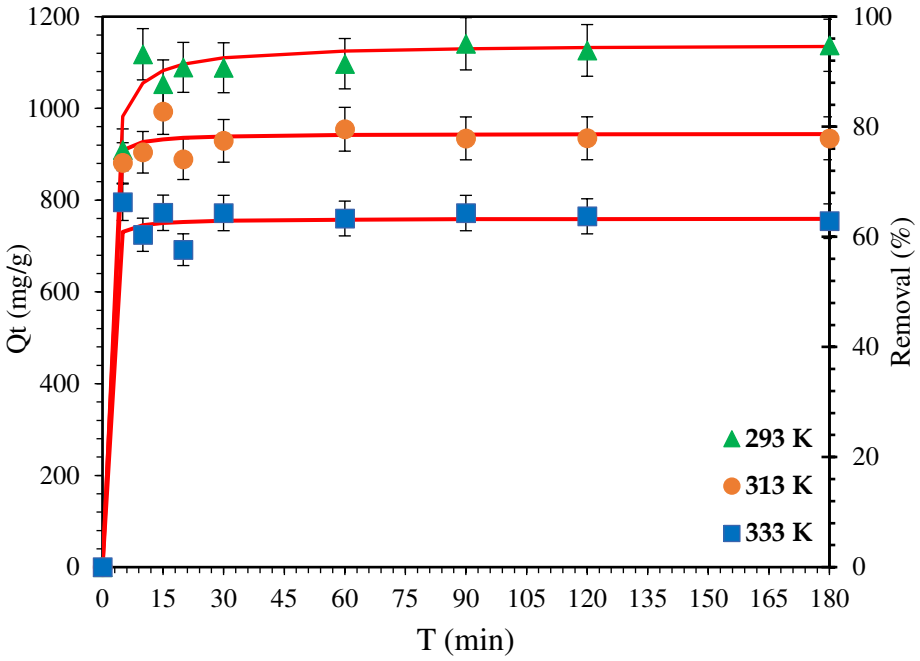

Fig. 10. Adsorption of bisphenol A onto AC-HP at different temperatures (pH 6.5; C_0=60mg/L; m= 0.01 g; agitation speed=200 rpm).

3.2.4. Adsorption Kinetics

The kinetic data of BPA adsorption on AC-HP was investigated at temperatures of 293, 313 and 333 K. The pseudo-second-order model is the most suitable for the BPA adsorption on AC-HP data because this model has a R^2 value close to 1 compared to pseudo-first-order model and the experimental adsorption capacity (1088 mg/g) was also close to the calculated adsorption capacity (1111.1 mg/g) (Fig. 11), suggesting a complex adsorption mechanism (Soni and Padmaja, 2014). The parameters depicting the adsorption procedures of BPA on AC-HP are listed in Table 6. Similar results with BPA interacting with various adsorbents have been reported by other researchers as well (Xu et al., 2012; Zhang et al., 2014).

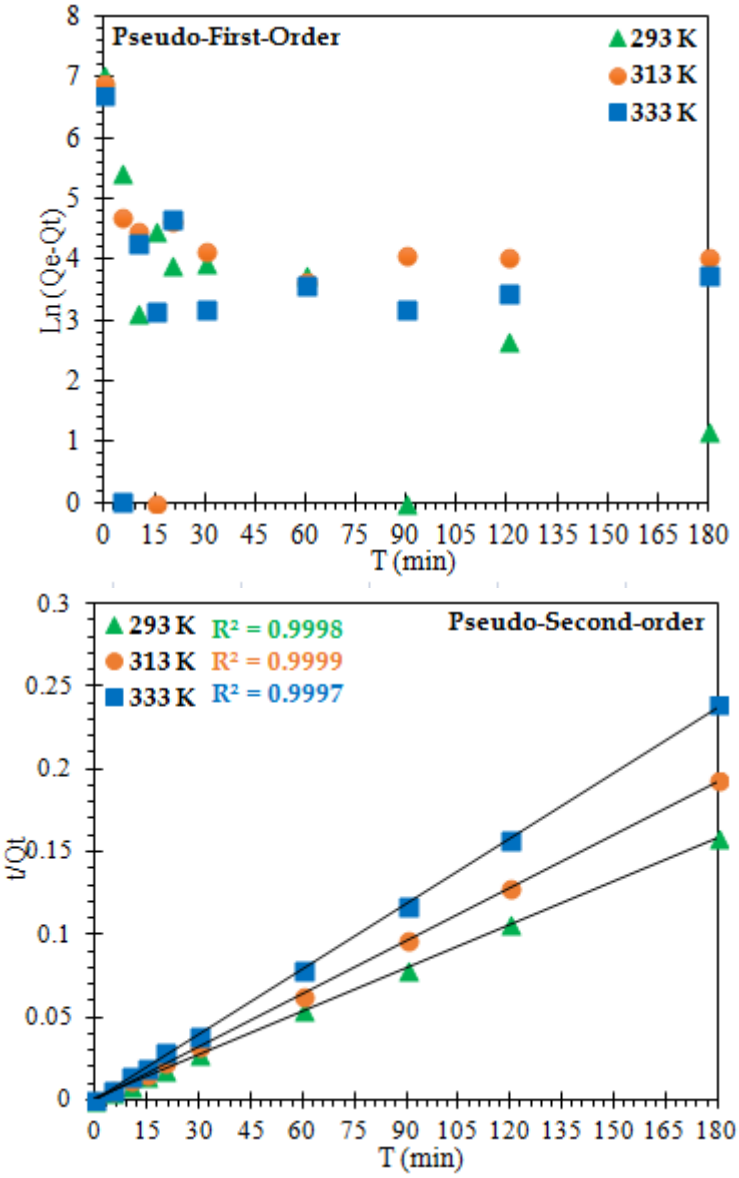

Fig. 11. BPA adsorption on AC-HP fitted by: pseudo-first-order kinetic equation and pseudo-second-order kinetic equation at different temperatures.

Table 6 Pseudo first-order and second-order parameters for adsorption of BPA onto AC-HP

	T(K)	$Q_{e,exp}$ (mg/g)	Pseudo-First-Order			Pseudo-Second-Order		
			$Q_{e,cal}$ (mg/g)	K_1 (1/min)	R^2	$Q_{e,cal}$ (mg/g)	K_2 (g/mg·min)	R^2
AC-HP	293	1088	132.97	0.058	0.1743	1111.1	0.001	0.9998
	313	929	65.93	0.005	0.2657	909.09	0.024	0.9999
	333	772	37.98	0.003	0.0245	769.23	0.028	0.9997

3.2.5. The intra-particle diffusion

To further understand the adsorption processes of BPA on AC-HP, we applied the Weber–Morris equation: $Q_t = K_i t^{0.5}$ (Weber, W.J. and Morris, 1963). Then, the Fig. 12 indicates that the intra-particle diffusion was also involved in the adsorption of BPA by AC-HP. However, the linear lines of the plots do not pass through the origin which indicate that the pore diffusion is, by all accounts, not the only rate-controlling step (Zou et al., 2016). Furthermore, from Fig. 12 it can be seen that there exist two particular regions: (1) the initial pore diffusion region because of the external mass transfer and the intra-particle diffusion region. The initial pore diffusion is a fast process that mainly depends on the surface area of AC-HP; (2) the intra-particle diffusion, starts to show slowing down of the diffusion and adsorption/desorption of BPA onto AC-HP is established (AL-Othman et al., 2012).

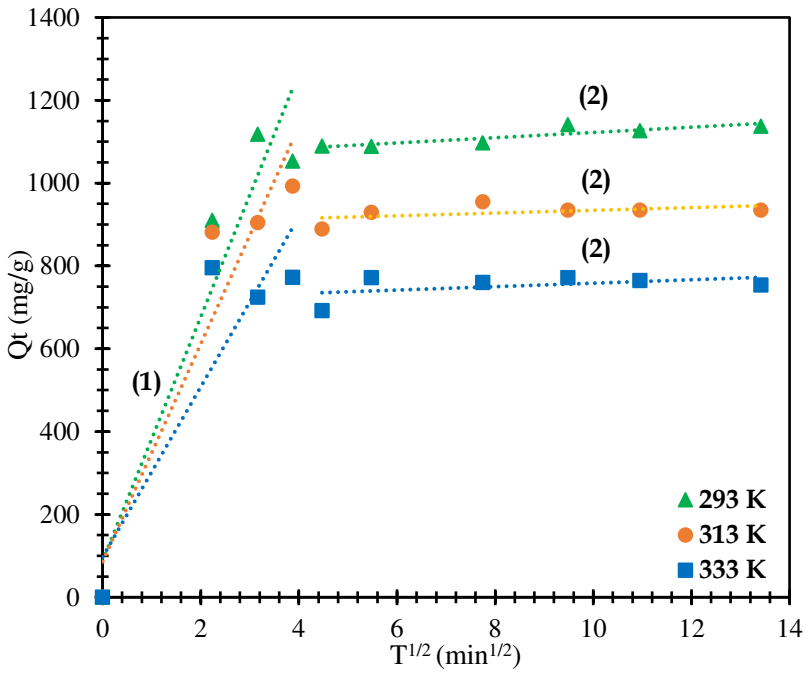

Fig. 12. Weber-Morris intra-particle diffusion model.

3.2.6. Adsorption isotherms

The adsorption experimental data of BPA on AC-HP were modeled Langmuir and Freundlich models, are listed in Table 7. On the basis of the R^2 values (0.95 for Langmuir and 0.80 for Freundlich model), the adsorption isotherm fitted slightly better with the Langmuir model (Fig. 13). As the Langmuir equation is derived under the assumption of monolayer coverage on the homogenous surface, the fitting results imply that monolayer adsorption rather than multilayer adsorption occurred. The maximum adsorption capacity decreased from 1250 mg/g at 293 K to 666.67 mg/g at 333 K. Furthermore, the R_L values at different temperatures were in the range of $0<R_L<1$, which indicates that the adsorption process of BPA on AC-HP was favourable. The n value was significantly higher than 1, suggesting a favorable adsorption system and heterogeneity of the AC-HP adsorption sites.

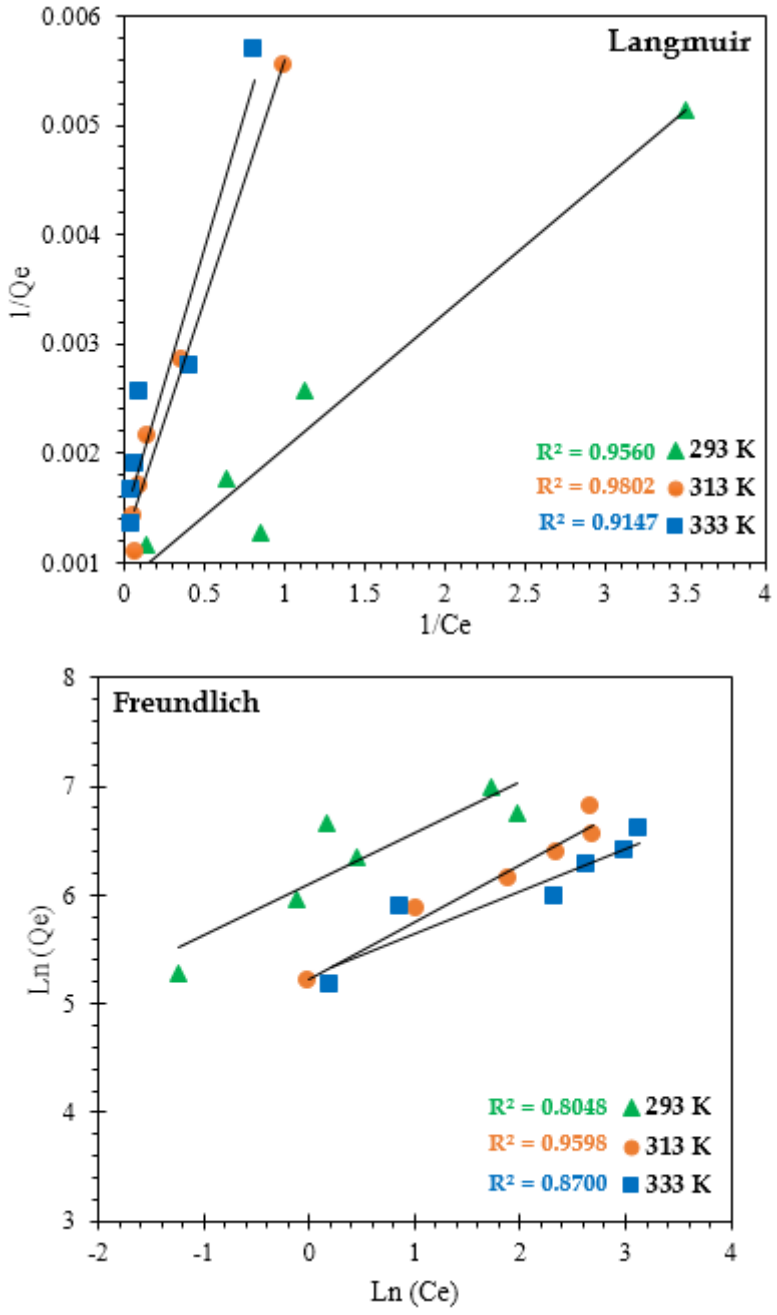

Fig. 13. Langmuir and Freundlich models for BPA adsorption onto AC-HP.

Table 8 shows a comparison of Q_{max} (mg/g) of BPA on various adsorbents reported in the literature. Since the Q_{max} (mg/g) of BPA adsorbed varies as a function of different parameters (temperature, pH, contact time, etc.), the experimental conditions applied in those studies are also listed in Table 8. It is visible that AC-HP has a higher adsorption capacity of BPA compared to the other studied materials.

Table 7 Parameters of Langmuir and Freundlich models of BPA onto AC-HP.

T (K)	Langmuir				Freundlich		
	Q_{max} (mg/g)	K_L (L/mg)	R_L	R^2	K_F (mg g^{-1}) (L $mg^{-1})^{1/n}$	n	R^2
293	1250.00	0.667	0.024	0.9560	440.72	2.258	0.8048
313	833.33	0.273	0.058	0.9802	185.84	1.899	0.9598
333	666.67	0.031	0.353	0.9147	190.55	2.541	0.8700

Table 8 Adsorption capacities of BPA of the prepared activated carbons compared to the literature datas.

Adsorbent	BET Surface Area (m^2/g)	Maximum Adsorption Capacity (mg/g)	Reference
AC-HP	1372	1250	Our study
AC purchased from Wako	1350	56.5	(Asada et al., 2004)
AC purchased from Takeda	1119	23.5	(Nakanishi et al., 2002)
As-grown CNTs	78	61.0	(Kuo, 2009)
Modified CNTs	95	70.0	(Kuo, 2009)
Graphene	327	181.6	(Xu et al., 2012)
Mesoporous carbon CMK-3	920	296	(Sui et al., 2011)
Activated carbon	1760	432.34	(Liu et al., 2009)
Hybrid material (Ph-MS)	750	351	(Kim et al., 2011)
Powdered-activated-carbon	-	771.2	(Li et al., 2014)
$CoFe_2O_4$/powdered-activated-carbon composite	-	727.2	(Li et al., 2014)

3.2.7. Thermodynamic parameters

The thermodynamic parameters of BPA adsorbed on AC-HP were studied by determining the effect of temperature on its removal. The thermodynamic parameters, ΔH°, ΔS° and ΔG° (presented in Table 9) were obtained by using the Van't Hoff and Gibbs-Helmholtz equations (Ouyang et al., 2015).

The R^2 value is higher than 0.98, indicating that the BPA adsorption data fitted well the Van't hoff equation (Fig. 14). The negative values of ΔG° at all temperatures indicate that

the adsorption of BPA on AC-HP was a thermodynamically feasible and its spontaneous process. At the same time, the values of ΔG° became more negative with decreasing the temperature, indicating a more efficient adsorption of BPA at lower temperatures. The value of ΔH° was negative, indicating the exothermic process of the BPA adsorption. The negative value of ΔS° reflected the decreased randomness at the solid (AC-HP)-liquid (BPA) interface during the adsorption process (Badruddoza et al., 2011). Furthermore, the adsorption process is supposed to proceed via physisorption, when the values of ΔG° are between 0 and -20 kJ/mol, while for chemisorption the values of ΔG° are generally between -80 and -400 kJ/mol (Phatthanakittiphong and Seo, 2016). In our study, the obtained ΔG° ranged between -9 to -12 kJ/mol, meaning that the adsorption of BPA by AC-HP is a physisorption process. The same result was also found for the BPA adsorption on graphene and reduced graphene oxide (Hosseini-Bandegharaei et al., 2010; Kwon and Lee, 2015; Xu et al., 2012).

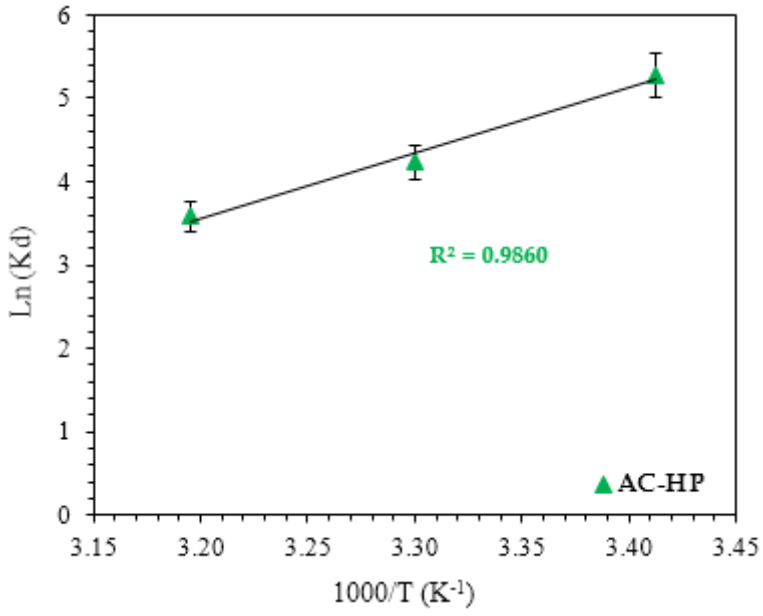

Fig. 14. Plot of Ln(K_d) vs. 1/T for thermodynamic parameters calculation for the adsorption of BPA on AC-HP.

Table 9 Thermodynamic parameters for the adsorption of BPA on AC-HP.

	ΔH° (J/mol)	ΔS° (kJ/mol K)	ΔG° (kJ/mol)		
			293 K	303 K	313 K
AC-HP	-64.806	-0.178	-12.872	-10.663	-9.336

3.2.8. Adsorption mechanism

Generally, the π-π interaction has been used to explain the mechanism of molecules with the C=C double bonds or benzene rings adsorbed on the surface of the carbonaceous material. This owes to organic molecules containing π electrons that interact with the π electrons of benzene rings of carbon material by means of the π-π electron coupling (Coughlin and Ezra, 1968). Since BPA, likewise, has benzene rings, it could be speculated that the main intermolecular force between BPA and AC-HP should be the π-π interaction. In addition, there were residual groups containing oxygen such as hydroxyl groups remaining in AC-HP, as shown by the FTIR measurement, which can form a hydrogen bond with the hydroxyl groups of BPA. Thus, we can expect that two kinds of AC-HP/BPA interactions might be responsible for the adsorption of BPA on AC-HP (Kim et al., 2011). One primary interaction was the π-π interaction between the benzene rings of BPA and AC-HP planes. The other one was hydrogen-bonding between the oxygen-containing groups contained both in BPA and AC-HP (Ersoz et al., 2004). In Fig. 15 the schematic representation of the π-π interaction and hydrogen-bonding between BPA and AC-HP is shown.

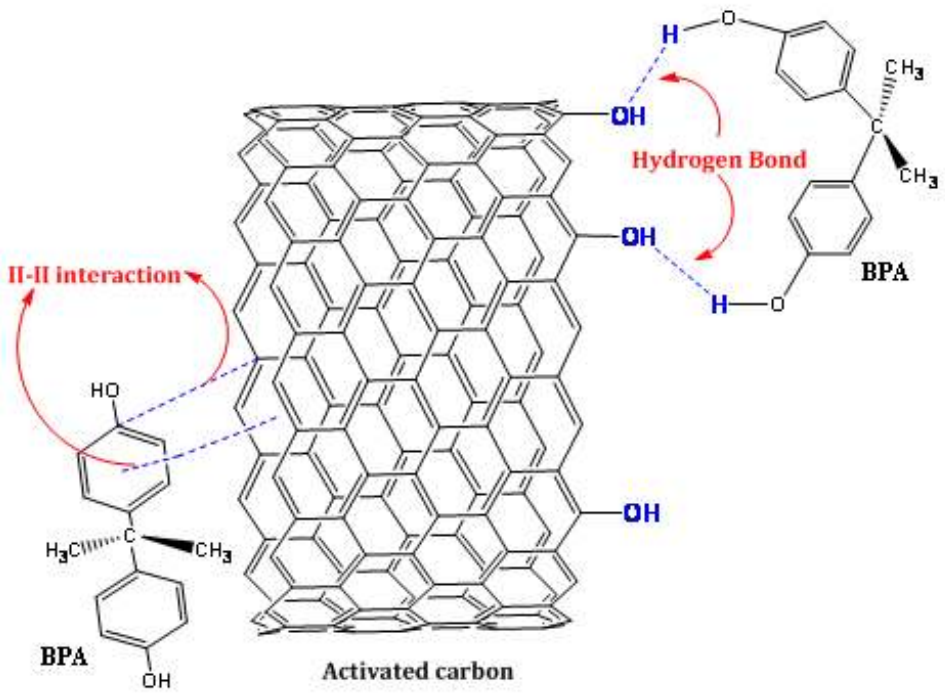

Fig. 15. Schematic representation of the π-π interaction and hydrogen-bonding between BPA and AC-HP.

In order to further understand the adsorption mechanism of BPA on AC-HP, the FTIR spectra of unused AC-HP and AC-HP after adsorption were compared. Fig. 16 reveals that several new peaks appear in the FTIR spectrum of AC-HP after the adsorption of BPA. These new peaks at 2800-3000 cm^{-1} and 500-1900 cm^{-1} are in accordance with the peaks from the FTIR spectrum of BPA and appeared with significant intensities, which indicates that a large amount of BPA has been adsorbed on the surface of AC-HP. Moreover, the stretching frequency of O-H groups was shifted from 3436 to 3239 cm^{-1}, which can be interpreted by hydrogen-bonding between hydroxyl groups contained both in BPA and AC-HP (Kim et al., 2011). The peak that belongs to the skeletal vibration of the aromatic C=C bonds also shifted from 1636 to 1620 cm^{-1} after adsorption, indicating the possibility of the π-π interaction between the benzene rings of BPA and AC-HP planes (Coughlin and Ezra, 1968). Consequently, the results obtained from FTIR spectroscopy show a new way

to demonstrate the presence of the π-π interaction and hydrogen-bonding between BPA and AC-HP.

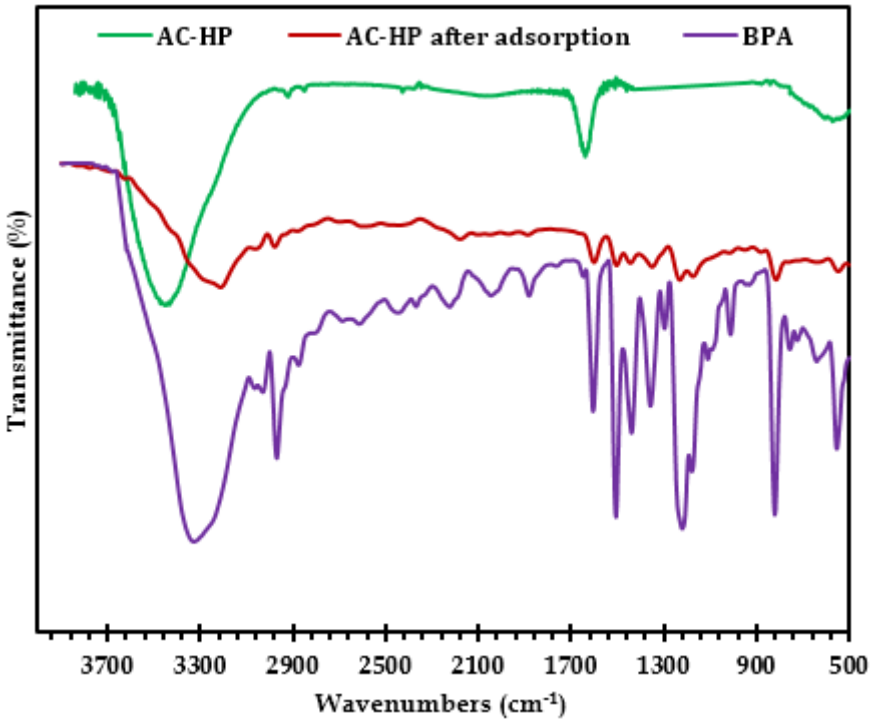

Fig. 16. FTIR spectra of AC-HP, BPA and AC-HP after BPA adsorption.

3.2.9. Regeneration and reusability

The regeneration and reusability of an activated carbon are very important characteristics to its practical application. In this study, the regeneration of the AC-HP after BPA adsorption was carried out by mixing BPA-loaded AC-HP with 20 mL of ethanol for 4 hours and then filtered and dried at 80 °C. Fig. 17 shows that the adsorption efficiency of AC-HP after 5 cycles was ~ 93 %. This result shows that AC-HP can be used repeatedly without a significant loss in the adsorption efficiency of BPA.

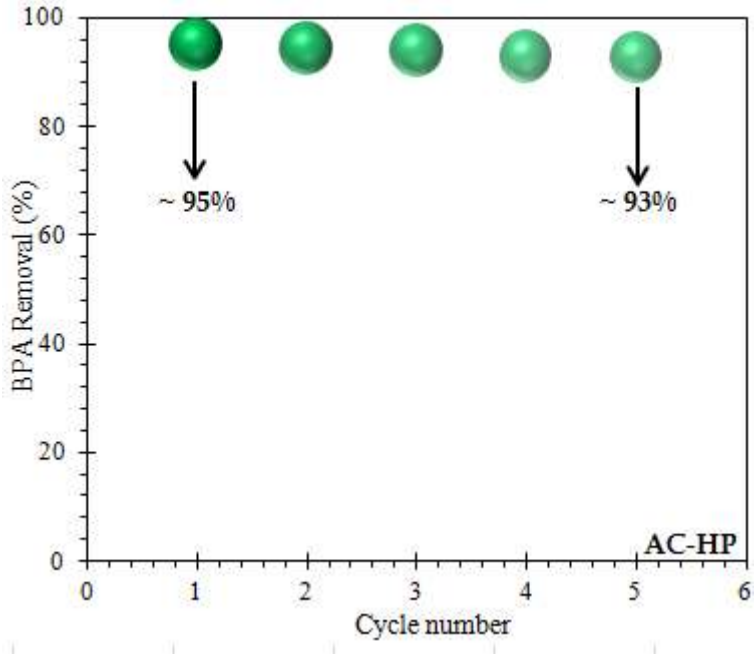

Fig. 17. The reusability of AC-HP for the adsorption of BPA (pH 6.5; C_0=60 mg/L; m=0.01 g; time= 180 min; stirring speed=200 rpm at 293 K).

4. Conclusion

The activated carbon (AC-HP) prepared from the argan nut shell using phosphoric acid is an efficient adsorbent for the BPA removal. The AC-HP showed a higher specific surface area (1372 m^2/g) compared to AC-Na (798 m^2/g), which was prepared by sodium hydroxide as activating agent. The adsorption tests of BPA were performed and the results indicated that AC-HP showed an excellent performance with a high adsorption capacity (1250 mg/g) at 293 K which is higher than other adsorbents reported in the literature. The adsorption kinetic data of BPA on AC-HP fitted well the pseudo-second-order kinetic. The outcomes of isotherm and thermodynamics studies indicated that the adsorption of BPA on AC-HP is exothermic and fitted well with the Langmuir isotherm. Moreover, AC-HP showed high adsorption efficiency of BPA (93 %) after 5 cycles of adsorption-regeneration. This work does not only open a new way to valorize argan nut shell, but also presents a simple sustainable approach to synthesize activated carbon,

which can be potentially used in many applications, such us energy storage, catalysis and environmental remediation, etc. However, these investigations are still ongoing.

Acknowledgments

The research leading to these results has received funding from the European Union Seventh Framework Programme [FP/2007-2013) under the grant agreement n° [PIRSES-GA-2012-317714]. No-Waste. The work has been supported also by the Academy of Finland via the AOPI-project (number 263580).

References

AL-Othman, Z.A., Ali, R., Naushad, M (2012) Hexavalent chromium removal from aqueous medium by activated carbon prepared from peanut shell: Adsorption kinetics, equilibrium and thermodynamic studies. Chem. Eng. J. 184, 238–247. doi:http://dx.doi.org/10.1016/j.cej.2012.01.048

Alum, A., Yoon, Y., Westerhoff, P., Abbaszadegan, M (2004) Oxidation of bisphenol A, 17β-estradiol, and 17α-ethynyl estradiol and byproduct estrogenicity. Environ. Toxicol. 19, 257–264. doi:10.1002/tox.20018

Asada, T., Oikawa, K., Kawata, K., Ishihara, S., Iyobe, T., Yamada, A (2004) Study of removal effect of bisphenol A and beta-estradiol by porous carbon. J. Heal. Sci. 50, 588–593. doi:10.1248/jhs.50.588

Badruddoza, A.Z.M., Tay, A.S.H., Tan, P.Y., Hidajat, K., Uddin, M.S (2011) Carboxymethyl-β-cyclodextrin conjugated magnetic nanoparticles as nano-adsorbents for removal of copper ions: Synthesis and adsorption studies. J. Hazard. Mater. 185, 1177–1186. doi:10.1016/j.jhazmat.2010.10.029

Bautista-Toledo, I., Ferro-García, M.A., Rivera-Utrilla, J., Moreno-Castilla, C., Vegas Fernández, F.J (2005) Bisphenol A removal from water by activated carbon. Effects of carbon characteristics and solution shemistry. Environ. Sci. Technol. 39, 6246–6250. doi:10.1021/es0481169

Bouchelta, C., Medjram, M.S., Bertrand, O., Bellat, J.-P (2008) Preparation and characterization of activated carbon from date stones by physical activation with steam. J. Anal. Appl. Pyrolysis 82, 70–77. doi:http://dx.doi.org/10.1016/j.jaap.2007.12.009

Chafik, T (2012) Nanoporous carbonated materials prepared from the shell of the argan fruit.

Coughlin, R.W., Ezra, F.S (1968) Role of surface acidity in the adsorption of organic pollutants on

the surface of carbon. Environ. Sci. Technol. 2, 291–297. doi:10.1021/es60016a002

Davydov, V.A., Rakhmanina, A. V, Agafonov, V., Narymbetov, B., Boudou, J.-P., Szwarc, H (2004) Conversion of polycyclic aromatic hydrocarbons to graphite and diamond at high pressures. Carbon N. Y. 42, 261–269. doi:10.1016/j.carbon.2003.10.026

Deng, H., Li, G., Yang, H., Tang, J., Tang, J (2010) Preparation of activated carbons from cotton stalk by microwave assisted {KOH} and {K2CO3} activation. Chem. Eng. J. 163, 373–381. doi:http://dx.doi.org/10.1016/j.cej.2010.08.019

Dias, J.M., Alvim-Ferraz, M.C.M., Almeida, M.F., Rivera-Utrilla, J., S??nchez-Polo, M (2007) Waste materials for activated carbon preparation and its use in aqueous-phase treatment: A review. J. Environ. Manage. doi:10.1016/j.jenvman.2007.07.031

El-Nabarawy, T., Petro, N.S., Abdel-Aziz, S (1997) Adsorption characteristics of coal-based activated carbons. II. Adsorption of water vapour, pyridine and benzene. Adsorpt. Sci. Technol. 15, 47–57. doi:10.1177/026361749701500105

Emmerich, F.G., Luengo, C.A (1993) Young's modulus of heat-treated carbons: A theory for nongraphitizing carbons. Carbon N. Y. 31, 333–339. doi:http://dx.doi.org/10.1016/0008-6223(93)90038-C

Ersoz, A., Denizli, A., Sener, I., Atilir, A., Diltemiz, S., Say, R (2004) Removal of phenolic compounds with nitrophenol-imprinted polymer based on pi-pi and hydrogen-bonding interactions. Sep. Purif. Technol. 38, 173–179. doi:10.1016/j.seppur.2003.11.004

Figueiredo, J.., Pereira, M.F.., Freitas, M.M.., Órfão, J.J (1999) Modification of the surface chemistry of activated carbons. Carbon N. Y. 37, 1379–1389. doi:10.1016/S0008-6223(98)00333-9

Freundlich, H.M.F (1906) Over the adsorption in solution. J. Phys. Chem. 57, 385–471.

Hadoun, H., Sadaoui, Z., Souami, N., Sahel, D., Toumert, I (2013) Characterization of mesoporous carbon prepared from date stems by {H3PO4} chemical activation. Appl. Surf. Sci. 280, 1–7.

doi:http://dx.doi.org/10.1016/j.apsusc.2013.04.054

Han, X., Wang, W., Ma, X (2011) Adsorption characteristics of methylene blue onto low cost biomass material lotus leaf. Chem. Eng. J. 171, 1–8. doi:http://dx.doi.org/10.1016/j.cej.2011.02.067

Hosseini-Bandegharaei, A., Hosseini, M.S., Sarw-Ghadi, M., Zowghi, S., Hosseini, E., Hosseini-Bandegharaei, H (2010) Kinetics, equilibrium and thermodynamic study of Cr(VI) sorption into toluidine blue o-impregnated XAD-7 resin beads and its application for the treatment of wastewaters containing Cr(VI). Chem. Eng. J. 160, 190–198. doi:http://dx.doi.org/10.1016/j.cej.2010.03.040

Howdeshell, K.L., Hotchkiss, A.K., Thayer, K.A., Vandenbergh, J.G., vom Saal, F.S (1999) Environmental toxins: Exposure to bisphenol A advances puberty. Nature 401, 763–764.

Ignat, M., Van Oers, C.J., Vernimmen, J., Mertens, M., Potgieter-Vermaak, S., Meynen, V., Popovici, E., Cool, P (2010) Textural property tuning of ordered mesoporous carbon obtained by glycerol conversion using SBA-15 silica as template. Carbon N. Y. 48, 1609–1618. doi:10.1016/j.carbon.2009.12.062

Ji, Y., Li, T., Zhu, L., Wang, X., Lin, Q (2007) Preparation of activated carbons by microwave heating {KOH} activation. Appl. Surf. Sci. 254, 506–512. doi:http://dx.doi.org/10.1016/j.apsusc.2007.06.034

Kim, Y.-H., Lee, B., Choo, K.-H., Choi, S.-J (2011) Selective adsorption of bisphenol A by organic–inorganic hybrid mesoporous silicas. Microporous Mesoporous Mater. 138, 184–190. doi:http://dx.doi.org/10.1016/j.micromeso.2010.09.007

Kolpin, D.W., Furlong, E.T., Meyer, M.T., Thurman, E.M., Zaugg, S.D., Barber, L.B., Buxton, H.T (2002) Pharmaceuticals, hormones, and other organic wastewater contaminants in U.S. streams, 1999–2000: A national reconnaissance. Environ. Sci. Technol. 36, 1202–1211.

doi:10.1021/es011055j

Kubilay, Ş., Gürkan, R., Savran, A., Şahan, T., 2007. Removal of Cu(II), Zn(II) and Co(II) ions from aqueous solutions by adsorption onto natural bentonite. Adsorption 13, 41–51. doi:10.1007/s10450-007-9003-y

Kuo, C.-Y (2009) Comparison with as-grown and microwave modified carbon nanotubes to removal aqueous bisphenol A. Desalination 249, 976–982. doi:http://dx.doi.org/10.1016/j.desal.2009.06.058

Kwon, J., Lee, B (2015) Bisphenol A adsorption using reduced graphene oxide prepared by physical and chemical reduction methods. Chem. Eng. Res. Des. 104, 519–529. doi:http://dx.doi.org/10.1016/j.cherd.2015.09.007

Laabd, M., Ait Ahsaine, H., El Jaouhari, A., Bakiz, B., Bazzaoui, M., Ezahri, M., Albourine, A., Benlhachemi, A., 2016. Congo red removal by PANi/Bi2WO6 nanocomposites: Kinetic, equilibrium and thermodynamic studies. J. Environ. Chem. Eng. 4, 3096–3105. doi:https://doi.org/10.1016/j.jece.2016.06.024

Langmuir, I (1916) The Constitution and Fundamental Properties of Solids and Liquids. Part I. Solids. J. Am. Chem. Soc. 252, 2221–2295. doi:10.1021/ja02268a002

Li, Z., Gondal, M.A., Yamani, Z.H (2014) Preparation of magnetic separable CoFe2O4/PAC composite and the adsorption of bisphenol A from aqueous solution. J. Saudi Chem. Soc. 18, 208–213. doi:http://dx.doi.org/10.1016/j.jscs.2011.06.012

Lillo-Ródenas, M.A., Lozano-Castelló, D., Cazorla-Amorós, D., Linares-Solano, A (2001) Preparation of activated carbons from Spanish anthracite: II. Activation by NaOH. Carbon N. Y. 39, 751–759. doi:http://dx.doi.org/10.1016/S0008-6223(00)00186-X

Liu, G., Ma, J., Li, X., Qin, Q (2009) Adsorption of bisphenol A from aqueous solution onto activated carbons with different modification treatments. J. Hazard. Mater. 164, 1275–

1280. doi:http://dx.doi.org/10.1016/j.jhazmat.2008.09.038

Marsh, H., Rodríguez-Reinoso, F (2006) {CHAPTER} 2 - Activated Carbon (Origins), in: Marsh, H., Rodríguez-Reinoso, F. (Eds.), Activated Carbon. Elsevier Science Ltd, Oxford, pp. 13–86. doi:http://dx.doi.org/10.1016/B978-008044463-5/50016-9

McKay, G., 1999. Pseudo-second order model for sorption processes. Proc Biochem. 34, 451.

McKendry, P (2002) Energy production from biomass (part 2): conversion technologies. Bioresour. Technol. 83, 47–54. doi:http://dx.doi.org/10.1016/S0960-8524(01)00119-5

Mohan, D., Sarswat, A., Singh, V.K., Alexandre-Franco, M., Pittman Jr., C.U (2011) Development of magnetic activated carbon from almond shells for trinitrophenol removal from water. Chem. Eng. J. 172, 1111–1125. doi:http://dx.doi.org/10.1016/j.cej.2011.06.054

Moreno-Castilla, C., Rivera-Utrilla, J (2001) Carbon Materials as Adsorbents for the Removal of Pollutants from the Aqueous Phase. MRS Bull. 26, 890–894. doi:10.1557/mrs2001.230

Muñoz-de-Toro, M., Markey, C.M., Wadia, P.R., Luque, E.H., Rubin, B.S., Sonnenschein, C., Soto, A.M (2005) Perinatal Exposure to Bisphenol-A Alters Peripubertal Mammary Gland Development in Mice. Endocrinology 146, 4138. doi:10.1210/en.2005-0340

Nakanishi, A., Tamai, M., Kawasaki, N., Nakamura, T., Tanada, S (2002) Adsorption characteristics of bisphenol A onto carbonaceous materials produced from wood chips as organic waste. J. Colloid Interface Sci. 252, 393–396.

Noh, J.S., Schwarz, J.A (1989) Estimation of the point of zero charge of simple oxides by mass titration. J. Colloid Interface Sci. 130, 157–164. doi:http://dx.doi.org/10.1016/0021-9797(89)90086-6

Ono, S (2000) Ministry of Health, Labour and Welfare (MHLW, Japan), in: Exposure and Behavior Researches of Endocrine Disrupting Chemicals in Tap Water. John Wiley & Sons, Inc. doi:10.1002/9780471462422.eoct344

Orfão, J.J.M., Antunes, F.J.A., Figueiredo, J.L (1999) Pyrolysis kinetics of lignocellulosic materials—three independent reactions model. Fuel 78, 349–358. doi:http://dx.doi.org/10.1016/S0016-2361(98)00156-2

Ouyang, K., Zhu, C., Zhao, Y., Wang, L., Xie, S., Wang, Q (2015) Adsorption mechanism of magnetically separable Fe3O4/graphene oxide hybrids. Appl. Surf. Sci. 355, 562–569. doi:http://dx.doi.org/10.1016/j.apsusc.2015.07.109

Phatthanakittiphong, T., Seo, G (2016) Characteristic evaluation of graphene oxide for bisphenol A adsorption in aqueous solution. Nanomaterials 6, 128. doi:10.3390/nano6070128

Pirilä, M., Saouabe, M., Ojala, S., Rathnayake, B., Drault, F., Valtanen, A., Huuhtanen, M., Brahmi, R., Keiski, R.L (2015) Photocatalytic Degradation of Organic Pollutants in Wastewater. Top. Catal. 58, 1085–1099. doi:10.1007/s11244-015-0477-7

Post, B (1975) X-ray diffraction procedures for polycrystalline and amorphous materials. Harold P. Klug and Leroy E. Alexander, John Wiley & Sons, New York (1974) pp. 960. $37.50. X-Ray Spectrom. 4, A18–A18. doi:10.1002/xrs.1300040415

Rivera-Utrilla, J., Sánchez-Polo, M., Gómez-Serrano, V., Álvarez, P.M., Alvim-Ferraz, M.C.M., Dias, J.M (2011) Activated carbon modifications to enhance its water treatment applications. An overview. J. Hazard. Mater. 187, 1–23. doi:http://dx.doi.org/10.1016/j.jhazmat.2011.01.033

Romero-Cano, L.A., Garc?a-Rosero, H., Gonzalez-Gutierrez, L. V., Baldenegro-P?rez, L.A., Carrasco-Mar?n, F (2017) Functionalized adsorbents prepared from fruit peels: Equilibrium, kinetic and thermodynamic studies for copper adsorption in aqueous solution. J. Clean. Prod. 162, 195–204. doi:10.1016/j.jclepro.2017.06.032

Selvaraj, K.K., Shanmugam, G., Sampath, S., Joakim Larsson, D.G., Ramaswamy, B.R (2014) GC–MS determination of bisphenol A and alkylphenol ethoxylates in river water from India and

their ecotoxicological risk assessment. Ecotoxicol. Environ. Saf. 99, 13–20. doi:http://dx.doi.org/10.1016/j.ecoenv.2013.09.006

Sing, K.S.W., Everett, D.H., Haul, R. a. W., Moscou, L., Pierotti, R. a., Rouquérol, J., Siemieniewska, T (1985) REPORTING PHYSISORPTION DATA FOR GAS / SOLID SYSTEMS with Special Reference to the Determination of Surface Area and Porosity (Recommendations 1984). Pure Appl. Chem. 57, 603–619. doi:10.1351/pac198557040603

Soni, H., Padmaja, P (2014) Palm shell based activated carbon for removal of bisphenol A: an equilibrium, kinetic and thermodynamic study. J. Porous Mater. 21, 275–284. doi:10.1007/s10934-013-9772-5

Suhas, Carrott, P.J.M., Ribeiro Carrott, M.M.L., Singh, R., Singh, L.P., Chaudhary, M (2017) An innovative approach to develop microporous activated carbons in oxidising atmosphere. J. Clean. Prod. 156, 549–555. doi:10.1016/j.jclepro.2017.04.078

Sui, Q., Huang, J., Liu, Y., Chang, X., Ji, G., Deng, S., Xie, T., Yu, G (2011) Rapid removal of bisphenol A on highly ordered mesoporous carbon. J. Environ. Sci. 23, 177–182. doi:10.1016/S1001-0742(10)60391-9

Tsai, W.-T., Lai, C.-W., Su, T.-Y (2006) Adsorption of bisphenol-A from aqueous solution onto minerals and carbon adsorbents. J. Hazard. Mater. 134, 169–175. doi:http://dx.doi.org/10.1016/j.jhazmat.2005.10.055

Udeye, S.T. and N.I. and J.T. and V (2009) Adsorption of Lead(II) and Cadmium(II) Ions from Aqueous Solutions by Adsorption on Activated Carbon Prepared from Cashew Nut Shells . Int. J. Chem. Mol. Nucl. Mater. Metall. Eng.

Vaghetti, J.C.P., Lima, E.C., Royer, B., Cardoso, N.F., Martins, B., Calvete, T (2009) Pecan Nutshell as Biosorbent to Remove Toxic Metals from Aqueous Solution. Sep. Sci. Technol. 44, 615–644. doi:10.1080/01496390802634331

Weber, W.J. and Morris, J.C., 1963. Kinetics of adsorption carbon from solutions. J. Sanit. Engeering Div. Proceedings. Am. Soc. Civ. Eng. 89, 31–60.

Wetherill, Y.B., Akingbemi, B.T., Kanno, J., McLachlan, J.A., Nadal, A., Sonnenschein, C., Watson, C.S., Zoeller, R.T., Belcher, S.M (2007) In vitro molecular mechanisms of bisphenol A action. Reprod. Toxicol. 24, 178–198. doi:http://dx.doi.org/10.1016/j.reprotox.2007.05.010

Xu, J., Wang, L., Zhu, Y (2012) Decontamination of bisphenol A from aqueous solution by graphene adsorption. Langmuir 28, 8418–8425. doi:10.1021/la301476p

Yamamoto, T., Yasuhara, A., Shiraishi, H., Nakasugi, O (2001) Bisphenol A in hazardous waste landfill leachates. Chemosphere 42, 415–418. doi:http://dx.doi.org/10.1016/S0045-6535(00)00079-5

Yoon, Y., Westerhoff, P., Snyder, S.A., Esparza, M (2003) HPLC-fluorescence detection and adsorption of bisphenol A, 17β-estradiol, and 17α-ethynyl estradiol on powdered activated carbon. Water Res. 37, 3530–3537. doi:http://dx.doi.org/10.1016/S0043-1354(03)00239-2

Zhang, Y., Cheng, Y., Chen, N., Zhou, Y., Li, B., Gu, W., Shi, X., Xian, Y (2014) Recyclable removal of bisphenol A from aqueous solution by reduced graphene oxide–magnetic nanoparticles: Adsorption and desorption. J. Colloid Interface Sci. 421, 85–92. doi:http://dx.doi.org/10.1016/j.jcis.2014.01.022

Zou, Z., Zhang, Y., Zhang, H., Jiang, C (2016) A combined H3PO4 activation and boron templating process for easy synthesis of highly porous spherical activated carbons as a superior adsorbent for rhodamine B. RSC Adv. 6, 15226–15233. doi:10.1039/C5RA23834J